Journal of Power Sources 190 (2009) 189–200

Contents lists available at ScienceDirect

Journal of Power Sources

journal homepage: www.elsevier.com/locate/jpowsour

Precious metal oxides for electrochemical energy converters: Pseudocapacitance and pH dependence of redox processes

P. Kurzweil*

University of Applied Sciences, Kaiser-Wilhelm-Ring 23, D-92224 Amberg, Germany

ARTICLE INFO

Article history:
Received 9 June 2008
Accepted 11 August 2008
Available online 22 August 2008

Keywords:
Platinum metal oxide
Hydrous RuO_2
Double-layer capacitor
Proton conductor
pH sensor
Water sensor

ABSTRACT

The mechanism of charge storage in hydrous platinum metal oxides is considered in more detail with respect to the pH dependence of redox capacitance for applications in double-layer capacitors, fuel cells, and pH sensors. An amorphous RuO_2 electrode is able to work like a pH glass electrode during the titration of hydrochloric acid with sodium hydroxide solution. It is shown that the proton exchange mechanism at a glass membrane can be reproduced by platinum metal oxide-hydrates bound in a polymer matrix. Hydrous RuO_2, obtained by alkaline precipitation or thermal decomposition from $RuCl_3$, as well as single crystal RuO_2, were characterized by TOF-SIMS, NMR spectroscopy, and electrochemical techniques. The proton conductivity of hydrous RuO_2 appears to be due to the dissociative adsorption of water and the formation of acidic OH groups in Ru(III,IV) cluster ions. Depending on the pH of the solution, the electrode potential is determined by the formal hydrogen oxidation or oxygen reduction in ruthenium cluster ions. During aging, the active Ru(III) surface sites are partially oxidized to Ru(IV).

1. Introduction

1.1. Ruthenium dioxide for supercapacitors

The pH dependence of capacitance at platinum metal oxides should give further insights into the charge storage mechanism for applications in supercapacitors [1–3], fuel cells, and novel pH sensors. Since the late 1970s mixed platinum metal oxides, coated on titanium supports, have been developed for dimensionally stable electrodes (DSA) for chloralkali electrolysis [4–6]. In the 1990s high-surface area RuO_2 was employed for supercapacitors working in aqueous solution. Then, *Dornier* (Daimler Group, Germany) started a car on a cold spring morning by the aid of an bipolar 30 V/65 F alkaline supercapacitor, containing electrodes made of ruthenium oxide-hydrate; $RuO_2{\cdot}xH_2O$, finely dispersed in a mixture of polyalcohols, was screen-printed on carbon fiber paper that was fixed on both sides of a bipolar plate of nickel [7,8]. *Pinnacle Research Institute* (USA) employed ruthenium oxide in diluted sulfuric acid; etched titanium sheets were repeatedly dip-coated in an alcoholic solution of $RuCl_3{\cdot}3H_2O$, followed by drying and pyrolysis at 300–350 °C [9].

In recent years, finely dispersed platinum metal oxides were coated on carbon particles or bound in polymers [10–12]. The importance of the water content of the $RuO_2{\cdot}xH_2O$ material became obvious [13] for the achievable pseudocapacitance $C(U) = dQ/dU$, which arises from kinetically inhibited redox processes at the metal oxide–electrolyte interface and depends strongly on frequency, temperature, and the applied voltage U. The "electrostatic" double-layer capacitance of the Helmholtz layer is always superimposed by the "faradaic" delivered charges Q caused by the battery-like redox steps involved in the potential-determining charge-transfer reaction across the interface.

Metal oxides such as RuO_2, IrO_2, PtO_2, PbO_2, and SnO_2, are mixed electronic and ionic conductors, having an oxygen defect stoichiometry. It is generally accepted [2,6] that the pseudocapacitance of a RuO_2 electrode is caused by overlapping, highly reversible, redox processes including Ru(IV) and a small amount of Ru(III). Water molecules (not shown in Eq. (1)) surround the ruthenium atoms and saturate the free valences.

$$\begin{aligned} &RuO_x(OH)_y + ze^- + zH^+ \rightleftharpoons \underset{IV}{RuO_{x-z}}(OH)_{y+z} \\ &\text{or simplified:}\quad \underset{IV}{RuO_2} + e^- + H^+ \rightleftharpoons \underset{III}{RuO(OH)} \end{aligned} \tag{1}$$

By dissociative adsorption of water, as proposed in Fig. 1(a), the RuO_2 surface is covered by a carpet of OH-groups. During anodic charging, protons are displaced from the OH sites, and oxide sites

* Tel.: +49 9621 482 154; fax: +49 9621 482 145.
E-mail address: p.kurzweil@haw-aw.de.

0378-7753/$ – see front matter © 2008 Elsevier B.V. All rights reserved.
doi:10.1016/j.jpowsour.2008.08.033

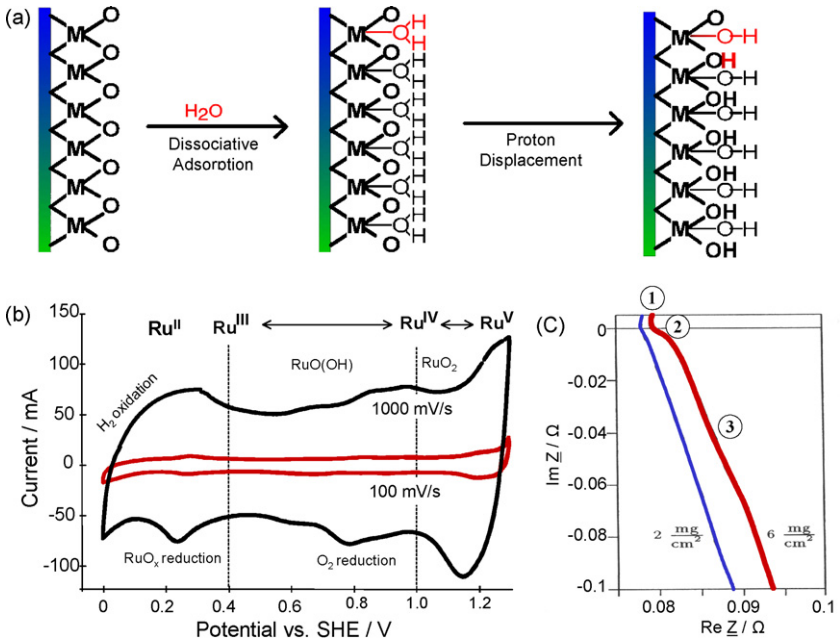

Fig. 1. (a) Mechanism of the redox capacitance of platinum metal oxides in aqueous solution. (b) Cyclic voltammogram of a RuO_2 electrode at different scan rates: $I = Cv$. Results of Section 3 are included. (c) ac impedance spectra of a cell of two RuO_2/Ni electrodes with different mass of metal oxide coating: 1 = electrolyte resistance, 2 = grain boundary resistance, 3 = diffusion impedance. *Note*: the mathematical convention of impedance.

are formed.

$$[\mathrm{Ru}]\text{–}(\mathrm{H_2O}) \rightleftharpoons [\mathrm{Ru}]\text{–}\mathrm{OH^-} + \mathrm{H^+}$$
$$\mathrm{OH^-(lattice)} \rightleftharpoons \mathrm{O^{2-}(lattice)} + \mathrm{H^+} \quad (2)$$
$$\mathrm{OH^-}_{(i)} + \mathrm{O^{2-}}_{(ii)} \rightleftharpoons \mathrm{O^{2-}}_{(i)} + \mathrm{OH^-}_{(ii)}$$

Actually, a RuO_2 film, weighed with a quartz crystal microbalance, during anodic charging, loses a mass of 56.3 u per electronic charge, which corresponds roughly to $[H(H_2O)_3]^+$ (mass 55) according to Eq. (2) [2]. Thoughts of a bulk diffusion process including H_3O^+ species were suggested already in 1978 [5]. Later the low activation energy of 4–5 kJ mol^{-1} for the charge storage in RuO_2 electrodes was attributed to proton diffusion via a Grotthus-type hopping mechanism.

The exact chemical nature of the Ru(III) and Ru(IV) species, and probably Ru(II) and Ru(V) and higher oxidation states, causing the highly reversible redox activity, shown in the cyclic voltammogram in Fig. 1(b), is still unknown. Reducing agents such as ascorbic acid and Fe^{2+} damage the reversibility both of RuO_2 anodes and cathodes, and reduce the usable voltage window of about 1.5 V considerably [7]. Solutions of $RuCl_3 \cdot 3H_2O$ can be reduced electrochemically to pink $[Ru(H_2O)_6]^{2+}$ ions, which again are quickly oxidized to yellow $[Ru(H_2O)_6]^{3+}$ by oxygen, or less fast by the decomposition of water. Ru(II), with hydrogen bound side-on, works as a proton source, $[Ru(H_2O)_5(H_2)]^{2+} \rightarrow [Ru(H_2O)_5H]^+ + H^+$ [15].

The protons (or hydroxide sites), formed by dissociative adsorption of water, can penetrate into the porous electrode material and stay in the electrochemical equilibrium with the surrounding solution. Accordingly, the impedance spectrum in Fig. 1(c) shows a diffusion branch at low frequencies which depends clearly on the thickness of the active layer [1]. The voltammetric charge increases with rising RuO_2 mass until the film gets too thick; solid-phase redox reactions in the bulk material contribute by an amount of about 7% to the overall capacitance [6]. In particles with sizes of >30 nm, therefore, most of the charge capability will remain unused in the particle core [2].

1.2. Ruthenium dioxide as a pH probe

Hydrogen electrodes (Pt/H_2), chinhydron electrodes, and antimony electrodes (Sb/Sb_2O_3) are state-of-the-art for pH measurements. Although pH probes based on, e.g. PbO_2, SnO_2, ZrO_2, Ta_2O_5, RuO_2 and IrO_2 have been proposed in literature, e.g. [14], metal oxide pH sensors are not available commercially. According to Eq. (1), a RuO_2 electrode should work as a pH sensor in aqueous solutions. The NERNST equation for the Ru^{IV}/Ru^{III} reduction potential reads therefore:

$$E = E^0 - \frac{RT}{F} \ln \frac{a(\mathrm{Ru^{III}})}{a(\mathrm{Ru^{IV}})a(\mathrm{H^+})} = E^0 - \ln 10 \frac{RT}{F} \left(\mathrm{pH} + \log \frac{a(\mathrm{Ru^{III}})}{a(\mathrm{Ru^{IV}})} \right) \quad (3)$$

At 25 °C, and nearby equal activities of Ru(III) and Ru(IV), which approach $a = 1$ in the solid state, the electrode reduction potential should therefore drop in increasingly alkaline solution.

$$E = E^0 - 0.059\,\mathrm{pH} \quad (4)$$

The thermodynamically calculated standard potential of the redox reaction

$$2\mathrm{RuO_2} + 2\mathrm{H^+} + 2\mathrm{e^-} \rightleftharpoons \mathrm{Ru_2O_3} + \mathrm{H_2O} \quad (5)$$

equals $E^0 = 0.94$, but the measured potential in aqueous solution is about 0.75 V [6].

2. Experimental

Based on our initial assumption that hydrous platinum metal oxides might be proton conductors, we tried to gather more fundamental insights into the charge storage mechanism by help of spectroscopic, thermoanalytical, chemical and electrochemical methods. Our investigations try to answer the following questions:

1. Which redox reactions and phase changes dominate the pseudocapacitance of RuO_2 layers?

2. Do surface analytical methods suggest evidence for the proton conducting species in hydrous RuO_2?
3. Which conclusions about the long-term stability of RuO_2 supercapacitors can be drawn?

2.1. Sample preparation

In order to investigate the electroactive material free from binders and additives, RuO_2 was coated on a conductive metal substrate [8].

1. *Thermal spray pyrolysis*: an ink of commercial grade $RuCl_3 \cdot 3H_2O$ in isopropanol was painted on nickel sheets and heated in a furnace in air at 325 °C, 450 °C, and 600 °C for 5 h. The lowest temperature for the conversion of the chloride precursor into RuO_2 is obvious from thermogravimetric curves at about 325 °C. Typical films yield surface areas of 25–90 $m^2\,g^{-1}$, and capacitances around 50 $F\,g^{-1}$ in aqueous solutions. There is a residual content of bound chlorine in the amorphous rutile lattice.

$$2(RuCl_3 \cdot 3H_2O) + \frac{1}{2}O_2 \rightarrow 2(RuO_2 \cdot 1.5H_2O) + 6HCl$$

2. *Sol–gel method* (precipitation process): amorphous ruthenium(IV)-dioxide hydrate, $RuO_2 \cdot xH_2O$, was obtained by precipitation of ruthenium chloride using potassium hydroxide solution. The filtrate was washed several times in water and then dried carefully at 90 °C to yield a blue-black powder having a definite water content of about 7.5 mass%.

$$2RuCl_3 + 6KOH + \frac{1}{2}O_2 \rightarrow 2(RuO_2 \cdot 1.5H_2O) + 6KCl$$

Polymer bound metal oxide electrodes were fabricated by coating nickel plates with a thin layer of a mixture of metal oxide powder in commercial varnish based on epoxy resins and other polymers.

PtO_2 and IrO_2 electrodes were prepared by thermal decomposition of the hexachloro metal(IV) acids, H_2PtCl_6 and H_2IrCl_6, respectively, on nickel sheets.

2.2. Instrumentation

Atomic force microscopy (AFM): The topography of the electrodes was measured by the aid of the model "DimensionTM 3100" in the contact mode using a scan width of 20 μm. Thereby the fine metal tip at the end of the cantilever resides in permanent repulsive contact with the sample surface.

Visible light interferometry: A Veeco Wyko NT 1100 instrument was used in a scan window of 184 μm × 246 μm.

Electrochemical techniques: Impedance spectra were recorded using a Solartron FRA 1250 frequency response analyser. Cyclic voltammetry was conducted by the aid of a Solartron SI 1287 potentiostat. The cell comprised a RuO_2/Ni working electrode and a glassy carbon counter/reference electrode in aqueous solutions. The pH of the electrolyte was controlled by a commercial pH glass electrode (Schott), which was calibrated in buffer solutions from Merck.

Potentiometric *acid–base titration* curves were recorded by the aid of a Schott "Titroline Alpha". The voltage, with respect to an increasing volume of 0.1 M sodium hydroxide solution, was measured between a metal oxide working electrode and a glassy carbon counter electrode and a reversible hydrogen electrode (RHE), respectively.

The *equilibrium potential* of a RuO_2/Ni electrode (4 cm^2) after 24 h equals +0.12 V RHE and −0.68 V versus glassy carbon (at pH 1 at 25 °C in 0.1 M hydrochloric acid), and +0.85 V RHE and approximately 0.0 V versus glassy carbon (at pH 13 at 25 °C in 0.1 M sodium hydroxide), respectively. For the glassy carbon rod (2 mm diameter, 5 cm length), +0.81 V RHE (pH 1), and +0.84 V RHE (pH 14) were measured.

3. Results and discussion

3.1. Morphological aspects of capacitance

Microporous RuO_2 powders obtained by a sol–gel process show the highest capacitance values in supercapacitors. The question is, whether this high specific capacitance is rather due to the particle size distribution than a difference in electrochemistry between RuO_2 powders prepared from $RuCl_3$ by thermal decomposition in contrast to precipitation with KOH. For the following experiments, metal oxide electrodes were prepared without any organic binder to avoid any influence of the polymer system on the measured capacitance.

3.1.1. AFM micrographs

Atomic force micrographs of RuO_2 powders, prepared by thermal decomposition at different temperatures are shown in Fig. 2(a). Although significant differences in the topography do not appear, the 325 °C powder shows the largest surface roughness. The RuO_2 layer on the 325 °C sample is about 5.65 μm thick, which was controlled by visible light interferometry. The two peaks in the histogram, calculated over the displayed surface in Fig. 2(b), show the gaps (left) and heights (right) of the RuO_2 coating. The peak width reflects the range of surface roughness between 1 μm and 4 μm.

We conclude that nickel electrodes coated with thermally won RuO_2 have qualitatively the same topography in the submicrometer scale, which is characterized by a large amount of grain boundaries.

3.1.2. SEM micrographs

Under the scanning electron microscope, precipitated RuO_2 reflects a microporous powder with a range of pore sizes between 1 μm and 10 μm, which is a result of the aggregation of the nanoparticles during filtration and drying. The thermally prepared RuO_2 layers in Fig. 3 show a fissured surface which corresponds to the more or less rapid evaporation of the solvent. Distinct crystals cannot be distinguished; the layer is amorphous.

The X-ray microprobe analysis (EDX) of the sol–gel sample, proves <1% residual potassium in the powder. The powder prepared thermally at 325 °C contains <1% chlorine. However, residual chlorine from the $RuCl_3$ precursor was not detected in the 450 °C and 600 °C samples.

Crystalline RuO_2 produced by thermal treatment above 500 °C shows a most poor surface area. This is consistent to the XRD patterns of hydrous RuO_2 powders dried at different temperatures, as found earlier [7], that show the transition from the amorphous to the crystalline phase between 200 °C and 900 °C. With rising temperature, the lattice constants of the deformed elementary cell of amorphous powders approaches the literature values of the RuO_2 single-crystal, and the X-ray crystallite sizes increase by a factor of three. As well, specific capacitance of the RuO_2 layer increases the smaller are the particles—so that precipitated colloidal RuO_2 provides a geometrical advantage.

3.1.3. Capacitance

Crystalline RuO_2 shows poor capacitance both in cyclic voltammetry ($C = I/\nu$ at a given voltage U and scan rate $\nu = dU/dt$, see Fig. 1) and in ac impedance measurements, $C(\omega) = [\omega\,\mathrm{Im}\,Z(\omega)]^{-1}$. We assume that channels in the rutile lattice get too narrow for a considerable transport of protons (or their carriers) when the RuO_2

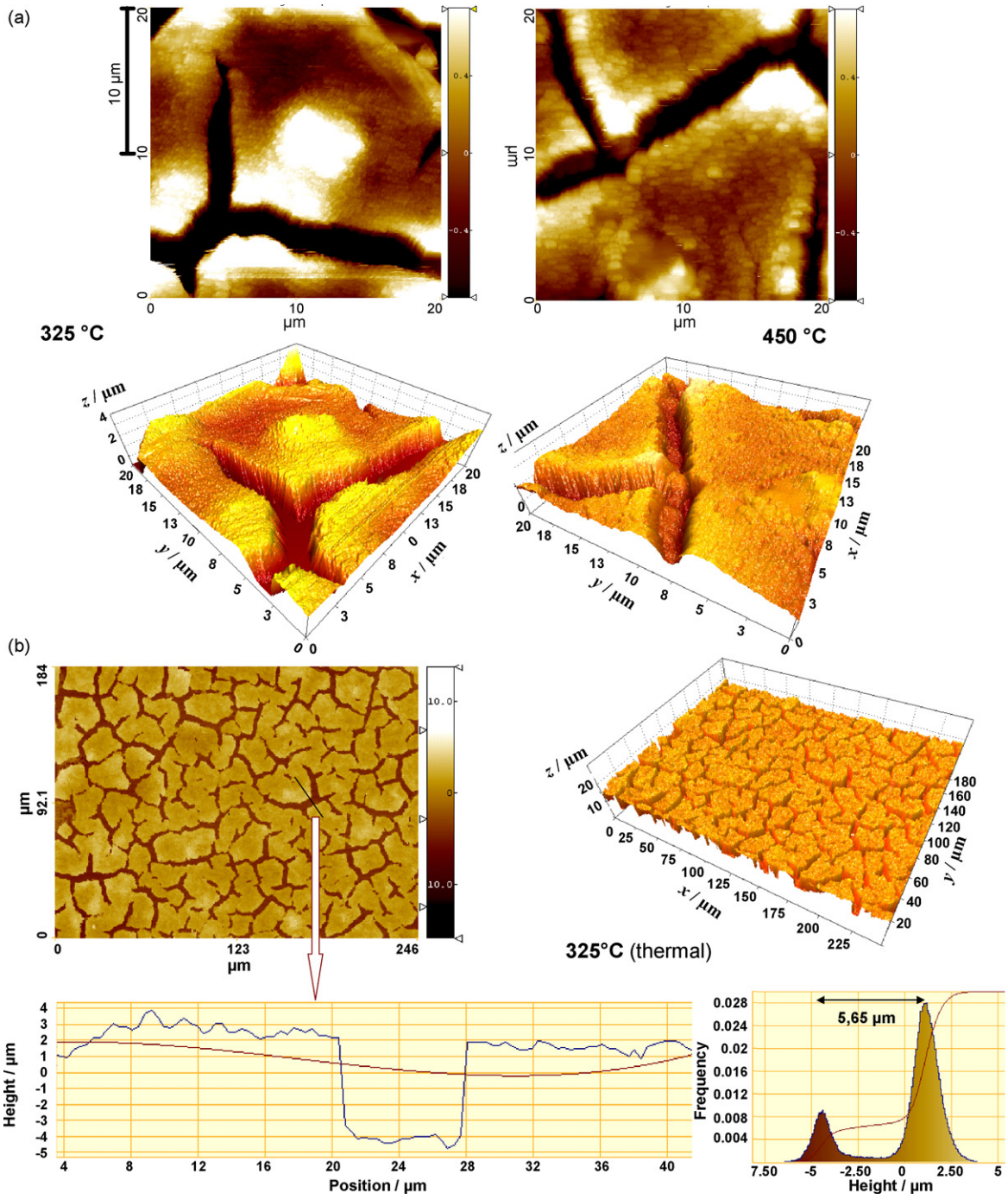

Fig. 2. (a) AFM-micrographs of RuO_2 electrodes prepared from $RuCl_3$ by thermal decomposition at 325 °C and 450 °C. Scan width 20 μm. (b) Visible light interferometry at the 325 °C RuO_2 electrode. Scan width 184 μm × 246 μm. Average layer thickness: 5.65 μm.

nanocrystallites grow by sintering and polycondensation processes during heat treatment and aging.

$$2(RuO_2{\cdot}1.5H_2O) \rightarrow (HO)_3Ru{-}O{-}Ru(OH)_3 \rightarrow \text{etc.}$$

In this case capacitance is determined by the "outer" surface area of the powder composite. Therefore, small particles providing more geometric surface area than the bigger particles, are most advantageous. Unfortunately, the interparticle contact at the grain boundaries causes an additional ohmic resistance in the supercapacitor (see region 2 in the impedance spectrum in Fig. 1) and makes increase the resistance along the electric pathway inside the electrolyte-filled pores (region 3). Moreover, the slope of the diffusion arc (region 3), apart from the 90° of an ideal capacitor, shows that the metal oxide–water interface is not totally blocking the electron charge transfer between the electrosorbed species and the electrode material.

The remaining question, however, is whether the electrochemical storage mechanism of the sol–gel powder differs fundamentally from that of thermally prepared RuO_2 particles.

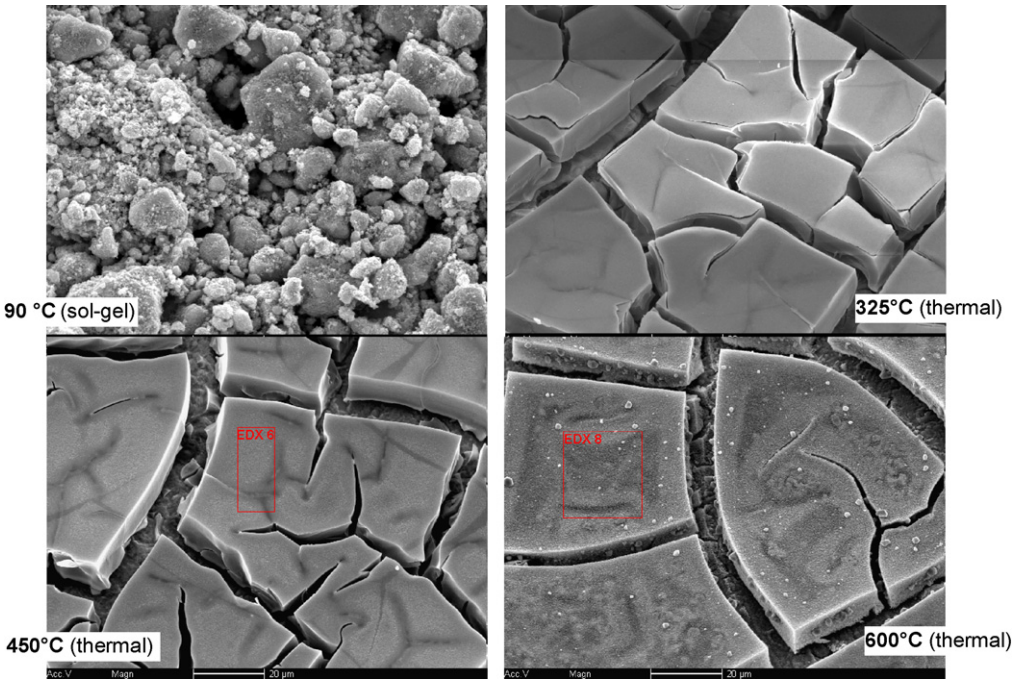

Fig. 3. SEM photographs in a 1000-times magnification of RuO_2/Ni electrodes prepared by coating with RuO_2 from a sol–gel process and drying at 90 °C (top left) and by thermal decomposition of an alcoholic $RuCl_3$ solution at different temperatures. No additives were used. An EDX analysis was made in the framed areas.

3.2. Surface chemical aspects of capacitance

In the following the charge storage mechanism at the RuO_2 surface is considered with respect to the chemical nature of the surface sites on amorphous RuO_2 powders and on RuO_2 single crystals. Time-of-flight secondary ion mass spectrometry (TOF-SIMS) was used to capture the first and second top atomic layers of the metal oxide without insight into the more or less stoichiometric bulk material.

3.2.1. Redoxactive species at the RuO_2 surface

The TOF-SIMS spectrum of sol–gel RuO_2 powder in Fig. 4 shows the striking signals of the three and four valent anions RuO_2^- and RuO_3^-, and smaller peaks of RuO^- and RuO_4^-, accompanied

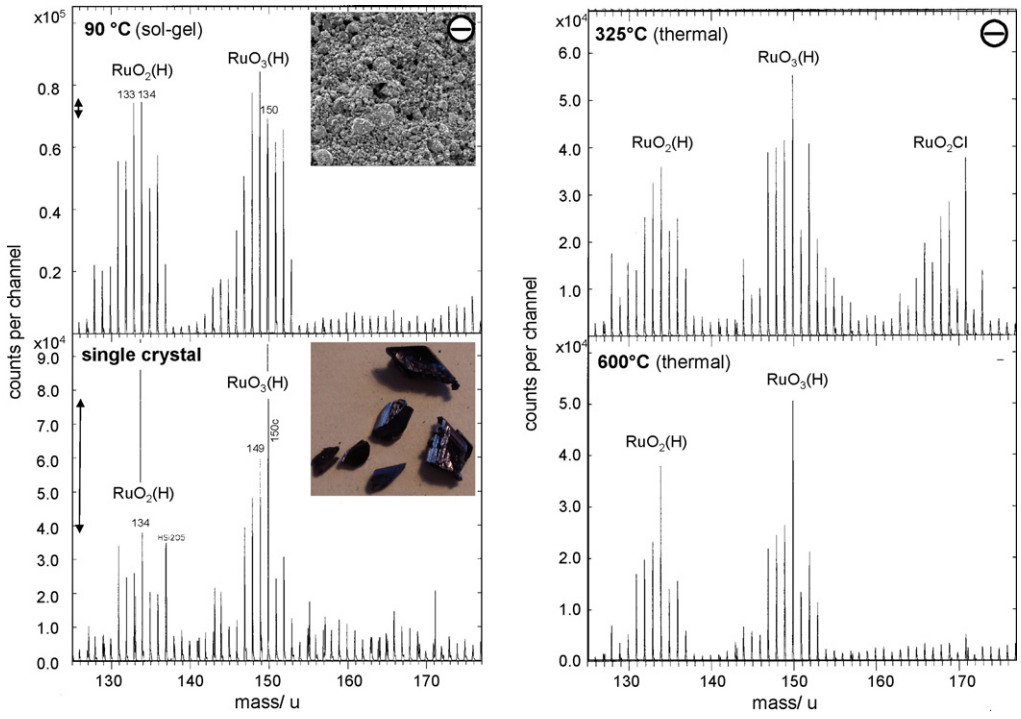

Fig. 4. TOF-SIMS spectra: comparison of ruthenium cluster anions from the surface of sol–gel particles, thermally prepared particles at different temperatures, and a RuO_2 single crystal. Note the peak ratios 149/150 and 133/134 as a measure for the acidity of the OH groups and ruthenium cluster ions, respectively.

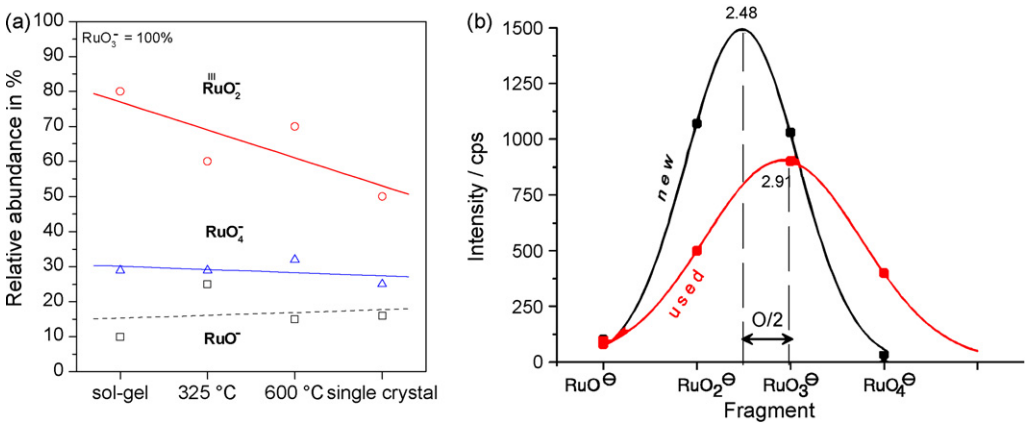

Fig. 5. (a): TOF-SIMS peak heights of RuO_n^- species relative to RuO_3^- (set 100%). (b) Relative oxidation of the RuO_2 surface between new and aged electrodes based on SIMS spectra.

by satellite peaks of the natural isotopic distribution. Additionally hydrogen-containing ions of the type $HRuO_n^-$ occur; which is not unusual at metal oxide surfaces generally. Negatively charged Ru_xO_y clusters follow at intervals of "RuO". Among the positive secondary ions, Ru^+ and $RuOH^+$ and clusters around mass 167 u were found. The sol–gel material is contaminated with potassium ions (due to the precipitation process with KOH), and negligible traces of Na, Mg, Ni, Al, Si, Ti, Mn, Cr, and organic acids.

The thermally prepared RuO_2 powder (325 °C) contains residual chlorine and Ru–O–Cl clusters, whereas the powders thermolyzed at higher temperatures are free of chlorine. As well, impurities of acid anions (SO_3^-, HSO_4^-, NO_2^-, NO_3^-, formiate, acetate) and traces of metals (Na, Mg, K, B, Al, Si, Ti, Cr, Mn) appear in the thermally prepared powders.

Generally, SIMS is able to detect stable structures only and multiple charged ions are not found normally. With increasing mass, the isotopic distribution gets so wide that overlapping structures complicate reliable conclusions. The dominant isotopes in nature are ^{102}Ru (31.6%, 101.9043 u), ^{104}Ru (18.7%), and ^{101}Ru (17.0%), followed by ^{100}Ru (12.6%), ^{99}Ru(12.7%), ^{96}Ru (5.5%), and ^{98}Ru (1.9%). Mass 133.9 u corresponds therefore to $^{102}RuO_2$, and mass 134.9 u to ^{102}RuO(OH), mass 149.9 u to $^{102}RuO_3^-$.

Qualitatively, a RuO_2 single crystal surface shows the same TOF-SIMS spectrum as the sol–gel powder. The relative amount of hydrogen containing oxides, $HRuO_n^-/RuO_n^-$, equals roughly 0.6 in all samples irrespectively of the route of preparation of the powders. A closer view at the peak heights, in Fig. 5(a), reveals a RuO_2^-/RuO_3^- ratio of 80% (sol–gel), 60% (325 °C sample), 70% (600 °C), and 50% (single crystal). RuO^- and RuO_4^- are less important in all samples.

According to certain SIMS theories, the peak ratios of a series of metal oxide anions (MO_1^-, MO_2^-, MO_3^-, and so on) hint at the actual mean oxidation state on the sample surface. On a pure quartz surface, as well, species occur such as $(H)SiO_2$, $(H)SiO_3$ and $(H)Si_2O_5$ anions. If we attributed the most intensive signal, $(H)RuO_3^-$ at mass ~150 u, to the dominating Ru(IV) state, and $(H)RuO_2^-$ (mass ~134 u) to Ru(III), then the actually measured redox capacitance would directly reflect the Ru(III)/Ru(IV) ratio on the electrode surface. In the sol–gel sample only, the strongest mass peaks at 133 u and 149 u might be attributed to the predominant Ru(III) and Ru(IV) species minus a proton. We conclude that the sol–gel RuO_2 contains the highest amount of proton conducting Ru(III), according to Eq. (2), followed by the thermally prepared samples.

3.2.2. Surface oxidation by aging

The SIMS spectra of RuO_2/Ni electrodes after extended life tests in supercapacitors [7] show that the intensities of the $[RuO_n]^-$ fragments are shifted from $n = 2.5$ to 2.9, i.e. by nearly half of an oxidation state compared to virgin electrodes. The aged sample shows a wider distribution of oxidation states; whereas cluster cations related to Ru_2^+, Ru_2O^+ and Ru_3^+ disappear more and more during aging. The depth profiles down to three monolayers differ by about 10% from the surface spectra. Although the absolute stoichiometry of ruthenium can hardly be determined exactly by SIMS, this qualitative result reveals the slow oxidation of the surface during long time operation at high current densities. Ru(III) sites are oxidized to Ru(IV), and higher oxidation states. We observed orange ruthenates(VI) as corrosion products in alkaline solution, which is consistent to the fact that the Ru(IV) cannot be oxidized without a burst of the structure, i.e. a transition of the octahedral to the tetrahedral coordination.

We conclude that the RuO_2 surfaces ages by partial oxidation, especially characterized by a loss of Ru(III) surface sites. The latter have been shown above to be essential for the dissociative adsorption of water involving proton conductivity.

3.2.3. Solid-state nuclear magnetic resonance

We tried to prove the proton conductivity of hydrous RuO_2 powders by help of the 300 MHz ^{1}H MAS-NMR-spectra [7] in Fig. 6.

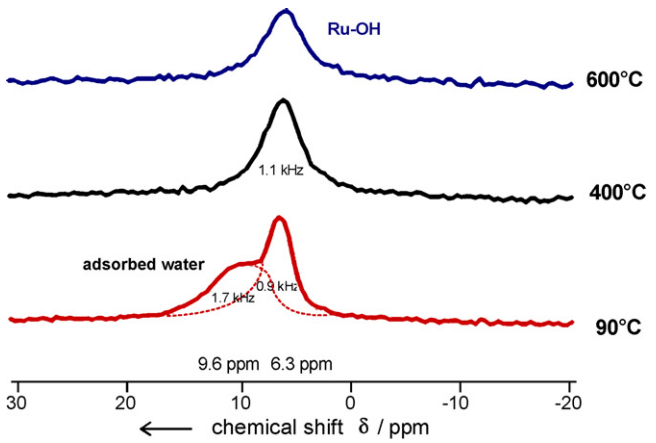

Fig. 6. ^{1}H MAS solid-state NMR spectra of hydrous RuO_2 powder, prepared by alkaline precipitation, and dried at different temperatures. The frequencies denote the linewidth at half-height.

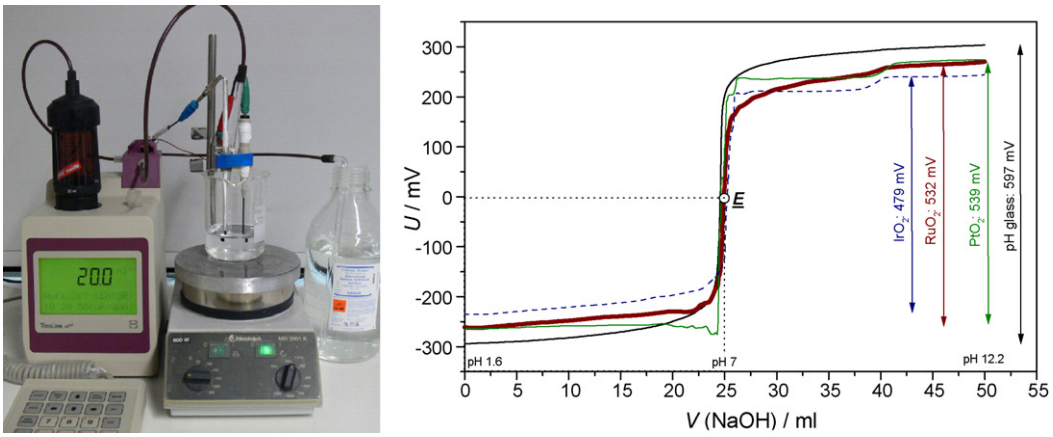

Fig. 7. Potentiometric titration of 0.025 M hydrochloric acid with 0.1 M sodium hydroxide solution by help of metal oxide electrodes (coated on nickel sheets). The counter/reference electrode was a glassy carbon rod. For the purpose of comparison, the curves were shifted into the voltage range of a commercial glass electrode (SCHOTT), and therefore intersect in the same point *E* (0 V).

There are hints at two sorts of protons: protons in adsorbed water (9.6 ppm), and protons in OH groups. The solid-state ^{1}H NMR spectra give no evidence for protons near paramagnetic centers (such as ^{99}Ru and ^{101}Ru), i.e. there are no Ru–H bonds in the $RuO_2{\cdot}xH_2O$ powder. Hence, protons must be coupled to oxygen sites such as in OH groups or at O bridges between Ru atoms. Adsorbed water disappears on heating (just as capacitance does), whereas protons bound in OH-groups are still observable in powders dried at 600 °C. Similar to silicagels, adjacent OH-groups might condense and form Ru–O–Ru bonds, which are not able to bind protons (or their carriers)—and consequently specific capacitance falls. The proton-conducting solid electrolyte "RuO(OH)" seems to attract and separate water from the electronic conductor "RuO_2". We imagine the hydrogen transport through the oxide like a movement of the RuO(OH)/RuO_2 interface, assuming a principal analogy to the nickel hydroxide electrode [16]. Under oxidizing conditions protons are removed from the OH sites according to Eq. (2).

We conclude that water plays the role of a carrier for the proton in RuO_2 (vehicle mechanism), which is consistent to the proton displacement model in Fig. 1. The OH-groups should be the more acidic the smaller is their number, if some analogy with silicagels is assumed. Without water present, considerable proton mobility and Ru(III) oxidation cannot happen.

3.3. The pH dependence of redox capacitance

With respect to Eq. (3), a RuO_2 electrode should be a more or less linear indicator for the actual pH value.

3.3.1. Screen-printed ruthenium dioxide as a pH probe

We found that a RuO_2 electrode is able to work like a pH glass electrode during the titration of hydrochloric acid with sodium hydroxide solution. A commercial glass electrode single-rod measuring cell passes a voltage range from −294 mV to +304 mV when applied between pH 1.6 and 12.2. The slope of 57 mV/pH at 20 °C fulfils the NERNST equation, and the endpoint of titration was reached at a voltage of 3 mV. Qualitatively the same shape of the potentiometric characteristics with a sensitivity of 50 mV/pH is obtained by hydrous RuO_2, which was prepared by a sol–gel process, bound in a polymer matrix (alkyd resin), and coated on a nickel sheet. Fig. 7 shows the acid–base titration curve of the RuO_2/Ni electrode—in comparison with a commercial glass electrode and thermally prepared metal oxide electrodes. PtO_2/Ni provides 51 mV/pH, and IrO_2 45 mV/pH.

The RuO_2 content in the print layer is most important for the measured voltage and the electrochemical properties of the electrode (Fig. 8). The best pH sensitivity is achieved by a mixture of 20% ruthenium oxide-hydrate in the polymer matrix. The RuO_2 powder was prepared by a sol–gel process according to EP 0 622 815 and contained 7.2% absorbed and bound water. In aqueous solutions of hydrochloric acid, the measured potential difference between the RuO_2 probe and a glassy carbon counter electrode clearly reflects the pH value. The voltage jump between pH 1.6 and 12.2 equals 532 mV, in contrast to a plain nickel sheet (176 mV) and a resin layer without metal oxide (346 mV). The average thickness *d* of the RuO_2 layer was 30 μm, and the active mass was 1.7 mg cm^{-2}. According to $\rho d = m/A$, the density ρ of the porous metal oxide-resin layer equals approximately 0.6 g cm^{-3}. Ten repeated measurements with the same RuO_2 probe in new electrolyte were reproducible by 6 mV and the endpoint of titration was accurate to 30 mV. Using several RuO_2 sensors, fabricated in the same way, the voltage values during the first titration differed less than 10–20 mV. The stability during long-term measurements up to 200 h at different pH values is good (about ±20 mV). During aging of the sensor, the potential difference between pH 0 and 14 drops slowly, but the endpoint is displayed correctly.

In commercial pH buffer solutions (MERCK) at 30 °C, the measured voltage values do not clearly reflect the trend of increasing pH values, in the same way both for RuO_2 and PtO_2 electrodes. Cell voltage increases from pH 0 to 7, but decreased from pH 8 to 14. It

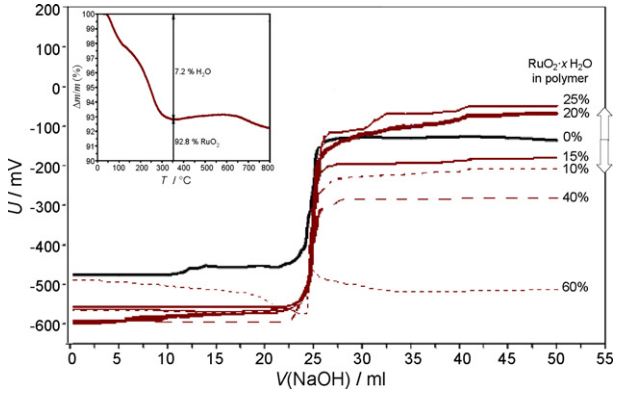

Fig. 8. Acid–base titration curves with polyester resin bound ruthenium oxide-hydrate on nickel sheets versus a glassy carbon rod (+0.81 V RHE, pH 1) at 30 °C. The sol–gel RuO_2 powder contained 7.2% water (see inset: thermogravimetric analysis).

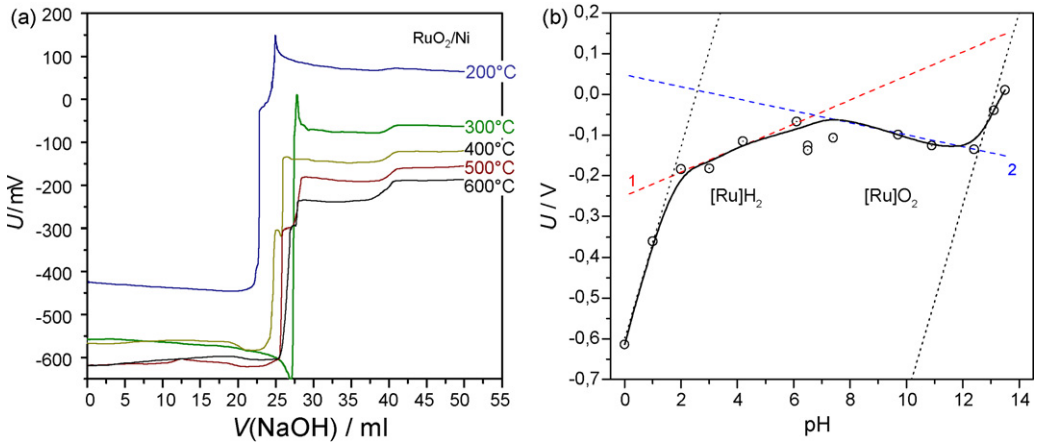

Fig. 9. (a) Potentiometric acid–base titration curves: dynamically measured potential of RuO_2/Ni electrodes prepared by thermal decomposition of $RuCl_3$ at different temperatures (versus glassy carbon, +0.81 V RHE). (b) Quasistationary potential of the RuO_2/Ni electrode (325 °C, 5 h; area 4 cm^2) versus glassy carbon in HCl and NaOH solutions at room temperature. Supporting electrolyte 8.9 g KCl per liter. Slope of the Nernst equation: 1 = (0.059/2) pH; 2 = –(0.059/4) pH.

is noteworthy that the measurements in distilled water and phthalate buffer (pH 7) are quite different due to the difference of ionic strength.

We conclude that the proton exchange mechanism at a glass surface can basically be reproduced by platinum metal oxide-hydrates. RuO_2 appears to be not a selective proton conductor, but its conductivity depends considerably on the ionic composition of the solution.

3.3.2. *Impact of binder and counter electrode*

Basically, the pH sensitivity does not depend on whether the metal oxides were prepared by thermal decomposition of salt solutions, or by alkaline precipitation (sol–gel process). However, sol–gel RuO_2 comes most close to the S-shaped characteristics of the glass electrode. The best "thermal" RuO_2 is obtained by decomposition of $RuCl_3$ on a nickel support at about 325 °C. As shown in Fig. 9(a), it yields the biggest jump of cell voltage, about 650 mV versus glassy carbon at pH 7, in comparison with samples thermolyzed at different temperatures. 200 °C is yet below the $RuCl_3 \rightarrow RuO_2$ transition.

Between pH 1.6 and 12.2, a cell of two more or less identical RuO_2/nickel electrodes exhibits a voltage change of about 100 mV, whereby the titration curve runs through an acute maximum at pH 7 (or exhibits a two linear sections with different slope) instead of the known sigmoidal shape. A cell of two more or less identical glassy carbon rod electrodes exhibits a nonlinear increase of voltage of about 200 mV during titration. A plain nickel sheet, as well as a thin layer of a polyester resin painted on nickel (see 0% RuO_2 in Fig. 8), causes a S-shaped pH characteristics versus the glassy carbon reference, having a small potential jump of about 350 mV near pH 7. Epoxy resin gives a jump of 430 mV at pH 7 in the most "beautiful" S-shape. More than 10% RuO_2 added to all resins disturb the pH sensitivity, especially as the trend of potential versus pH is reversed in alkaline solution (similar to 60% RuO_2 in Fig. 8).

We conclude that, for potentiometric measurements, RuO_2/nickel electrodes are at best combined with a glassy carbon counter electrode. RuO_2 powder, synthesized separately, can be bound by polyester and epoxy resin better than with other polymers (polyacrylate, polyurethane).

3.3.3. *pH-dependent electrode reactions*

The RuO_2 electrode is charged positively against a reversible hydrogen electrode; hence the open circuit voltage according to Eq. (1) should increase with rising pH.

$$U = U^0 + 0.059\mathrm{pH}$$

In Fig. 9(b) it is shown that the quasistationary potential of a RuO_2 electrode, after equilibration for 10 min, can be divided into two regions depending on pH. The electrolytes were diluted aqueous solutions of hydrochloric acid and potassium hydroxide, respectively. The ionic strength was defined by addition of 8.9 g KCl per liter solution. The pH values were controlled by a glass electrode.

1. In acid solution, as well as it is known for the hydrogen oxidation at a hydrogen electrode, the electrode potential increases with rising pH. Two electrons are involved in this process. We conclude that, only formally, hydrogen bound in RuO_2 is oxidized to hydronium ions. Actually, a proton is released by the dissociative adsorption of water.

$$[Ru^{III}]\text{–}O\text{–}[Ru^{III}] + H_2O \rightleftharpoons 2[Ru^{III}]OH \rightleftharpoons 2[Ru^{IV}]O^{II} + 2H^+ + 2e^-$$
$$\text{Formally}: \quad [Ru]H_2 \rightleftharpoons [Ru] + 2H^+ + 2e^-$$

2. In alkaline solution, as well as it is know for the oxygen reduction at an oxygen electrode, the electrode potential decreases with rising pH. The slope of the line calculated according to the Nernst equation indicates that four electrons are involved in this electrode reaction. We conclude that, formally, oxygen bound in RuO_2 is reduced to hydroxide ions. Actually, by the dissociative adsorption of water, formally, a proton is bound in the Ru(III) cluster, which is in accordance with Eq. (5).

$$2[Ru^{IV}]O^{II} + H_2O + 2e^- \rightleftharpoons [Ru^{III}]\text{–}O\text{–}[Ru^{III}] + 2OH^-$$
$$\text{Formally}: \quad [Ru]O_2 + 4e^- + 2H_2O \rightleftharpoons [Ru] + 4OH^-$$

The regions from pH 0 to 2 and from pH 12 to 14 are caused by electrode reactions, in which the electrochemical valency should equal about 0.25 in order to explain the slope of the Nernst line. This requires that the electron transfer is not linked to a single ruthenium atom, but to a cluster of atoms which is able to carry, for example, four electric charges. Indeed, the nature of Ru^{IV} in aqueous solution has already been described by a cluster ion such as $H_n[Ru_4O_6(H_2O)_{12}]^{(n+4)+}$, wherein n = 0, 1, 2, 3, 4 [17].

The cyclic voltammograms of a RuO_2 electrode against a glassy carbon counter/reference electrode at different pH values are

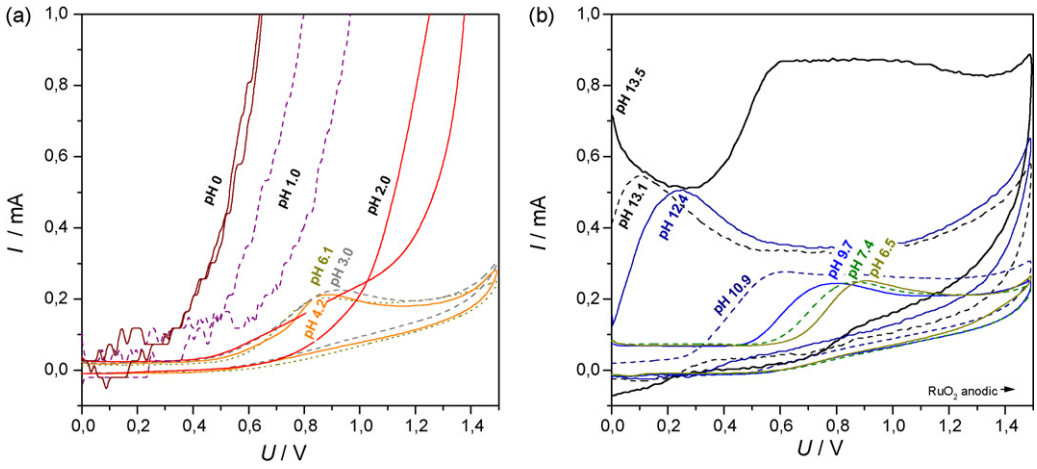

Fig. 10. Cyclic voltammograms of a cell of a RuO_2/Ni working electrode (4 cm^2, 325 °C, 5 h from $RuCl_3$) and a small glassy carbon rod counter/reference electrode in diluted hydrochloric acid (left) and sodium hydroxide (right). Scan rate: 20 mV s^{-1}. Supporting electrolyte: KCl (8.9 g l^{-1}).

shown in Fig. 10. The current peaks in the oxidation cycle at cell voltages <0.9 V increase proportional to the pH value (pH 6.5–9), and the redox potentials are shifted to more negative values. If the RuO_2 electrode is charged negatively the oxidation peak following the hydrogen evolution behaves, as well, proportional to the pH value. Conspicuously at pH 13.5, the high current of the overlapping redox couples demonstrates the power of supercapacitors based on RuO_2 in alkaline solution. At medium pH values, the anodic current at cell voltages between 1.0 V and 1.2 V reaches a minimum at pH ~6.5 to 7.

The glassy carbon counter electrode may be neglected in acid solution (<10 μA) as well as in alkaline solution (<20 μA at >~1.0 V). If a nickel counter/reference electrode is chosen, the cyclic voltammogram at positive potentials is coined by the nickel redox chemistry, whereas the RuO_2 cathode determines the CV at negative cell voltages.

3.3.4. Hydrogen sorption

If the above suggested charge storage mechanism of the RuO_2 electrode is correct, then we should be able to detect adsorbed hydrogen—at least bound in a ruthenium cluster.

Two identical RuO_2/Ni electrodes were fixed at constant distance in an arrangement of two gilt copper stamps, as shown in Fig. 11. The impedance spectra show a rise of capacitance in strongly acid and strongly alkaline solutions, respectively. Absolutely in the same way, if a plane nickel plate (same size) or a glassy carbon rod are chosen as the counter electrode, the trend of capacitance drops from pH 0 to 7, and then increases again from pH 7 to 14.

Gold is known to be an electrode material with negligible hydrogen sorption. In Fig. 11, it is shown that the reversed trend between cell voltage and pH value, which occurs above pH 7, can be shifted to about pH 2 by the aid of a plane counter electrode of gold. The total capacitance of the cell is dominated by the large capacitance of the rough RuO_2 electrode according to the following equation:

$$C = \left[\frac{1}{C_{RuO_2}} + \frac{1}{C_{Au}}\right]^{-1} \approx C_{RuO_2} \quad (6)$$

We conclude that the reversal of the trend of cell voltage versus pH is due to the hydrogen sorption (via cluster ions) at the RuO_2/Ni electrode. Hence, a RuO_2 electrode in acid solution or at a cathodic potential should work as a reversible hydrogen electrode.

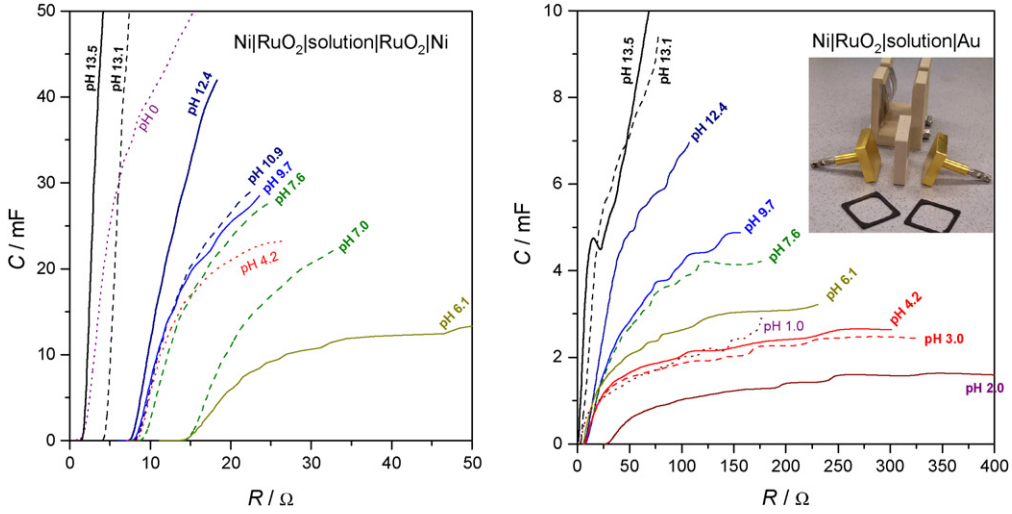

Fig. 11. Impedance spectra: cell capacitance versus cell resistance at frequencies between 1 kHz and 0.1 Hz. Left: a cell of two identical RuO_2/Ni electrodes (4 cm^2, 325 °C, 5 h from $RuCl_3$). Right: a rough RuO_2/Ni electrode versus a plane gold counter electrode of the same size. The electrolyte of diluted HCl and NaOH, respectively, contained 8.9 g KCl per liter of solution to define ionic strength. A dc bias was not applied.

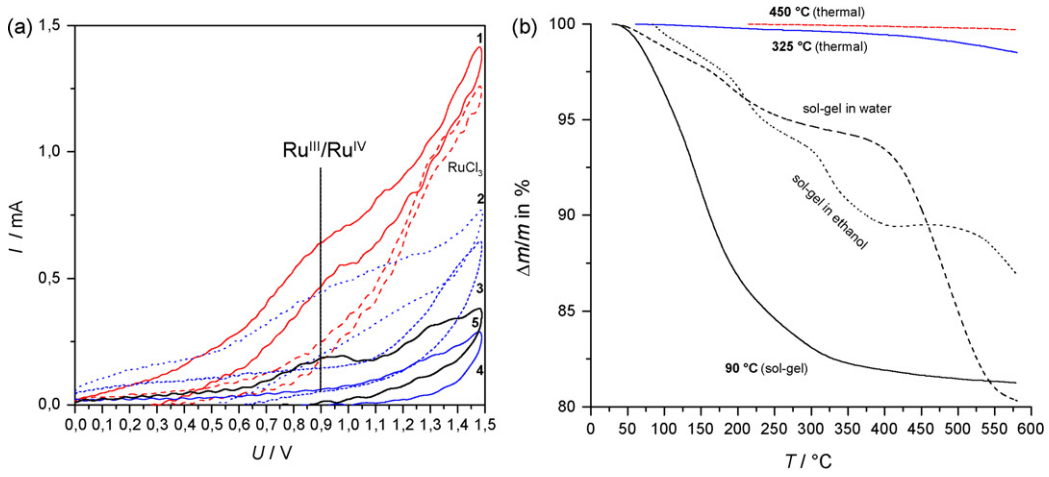

Fig. 12. (left) Cyclic voltamogramms of a cell of two glassy carbon electrodes during the sol–gel synthesis of RuO_2 from $RuCl_3$ in acetonitrile (dashed line); scan rate 20 mV s^{-1}, second cycle: 1 = 11 mmol KOH per liter of solution, 2 = 19 mmol l^{-1}, 3 = 26 mmol l^{-1}, 4 = 32 mmol l^{-1}, 5 = 38 mmol l^{-1}. (right) Thermogravimetric analysis of RuO_2 powders prepared by different methods. The 90 °C sample was dried in advance to remove bulk water.

A reference circuit of two glassy carbon electrodes can be used to compensate changes of temperature and ionic strength which effect the pH sensitivity of a RuO_2 pH electrode. The measured capacitance $C(\omega)$ of a RuO_2-glassy carbon cell is divided by the cell capacitance between a second glassy carbon electrode versus the first glassy carbon counter/reference electrode, C_{ref}; then the relative change of capacitance $(C - C_{ref})/C_{ref}$ indicates the pH value proportionally. The measuring frequency was chosen at 10 Hz advantageously in this three-electrode arrangement.

3.4. Characterization of RuO_2 precipitates

The above results illustrate that a certain amount of Ru(III) in the electrode material is essential for a high redox capacitance. Therefore, the products of the sol–gel synthesis of RuO_2 from $RuCl_3$ by precipitation with KOH solution were analyzed by the aid of electrochemical and spectroscopic methods with respect to the formation of Ru(III).

3.4.1. Electrochemistry of sol–gel RuO_2

In a glass vessel with two identical glassy carbon rod electrodes, a suspension of 0.15 g of $RuCl_3 \cdot 3H_2O$ (0.5 mmol) in 50 ml of a saturated solution of tetraethylammonium tetrafluoroborate in acteonitrile was titrated with potassium hydroxide solution (0.1 mol l^{-1}). The cyclic voltammograms in Fig. 12 show the stepwise precipitation and formation of $RuO_2 \cdot xH_2O$ when 6 ml portions of KOH are added without exclusion of air. The voltage window is gradually expanded and, finally, at about 0.9 V and 1.3 V, the redox processes appear which are typical of RuO_2 electrodes (cf. Fig. 1). The Ru^{III}/Ru^{IV} redox peak is achieved after adding of 38 mmol l^{-1} base.

3.4.2. Spectroscopic characterization of sol–gel RuO_2

Ruthenium dioxide was prepared by three methods:

1. Thermal decomposition of $RuCl_3$ at 325 °C (5 h); afterwards a second sample was dried at 450 °C (5 h).
2. Precipitation reaction of $RuCl_3$ with small portions of KOH (0.1 mol l^{-1}) until pH 7.5 is reached. The RuO_2 powder is centrifugated, washed in water twice, and dried at 90 °C for 24 h.
3. Precipitation of $RuCl_3$ in ethanolic KOH (0.1 mol l^{-1}) until pH 7.5 is reached. The RuO_2 is washed in ethanol and dried at 70 °C for 24 h.

The thermogravimetric analysis (Fig. 12) was conducted between room temperate and 600 °C at a heating rate of 10 K min^{-1}.

The IR spectra in Fig. 13 were recorded by the aid of a diamond ATR unit. The absorption due to the stretch vibration of H-bridged OH-groups above 3000 cm^{-1} is strongest for the RuO_2 precipitate, whereas the thermally prepared powders contain less adsorbed or chemically bound water.

To detect soluble ions, a slurry of 40 mg powder in 10 ml water or acetonitrile, respectively, was prepared and, after a sedimentation time of 8 min, measured in the UV–vis spectrometer between 190 nm and 1100 nm. In contrast to the "thermal" powders, the colloidal sol–gel sample forms a considerable amount of coloured ions in aqueous solution, which appear to be important for redox capacitance. The about a hundred times stronger absorption of $RuCl_3$ in water 400–700 nm is caused by the considerable solubility of Ru(III) in water.

3.5. Metal oxides in organic solution and long-term behaviour

Fig. 14 illustrates the completely different conduction mechanism of at thinly coated RuO_2/Ni electrode in contrast to a commercial activated carbon electrode (Gore). Whereas RuO_2 works best in aqueous solution, activated carbon is predestined for organic electrolytes. In a hybrid supercapacitor, based on the arrangement shown in Fig. 11, one of the two rough RuO_2 electrodes was replaced by a plane nickel plate. Cell capacitance is dominated by the rough electrode then, according to Eq. (6). The fundamental role of at least a trace of water for the redox capacitance of RuO_2 electrodes gets obvious by this experiment. The capacitance in organic electrolyte is mostly defined by the large surface area of the RuO_2 electrode, whereas in aqueous solution proton exchange (and water as the vehicle) at the RuO_2–electrolyte interface provides a jump of capacitance. Metal oxides electrodes having capacitances up to several hundred Farads per square centimeter may help to reduce the cost of such supercapacitors.

The self-discharge current of an alkaline RuO_2 supercapacitor increases with rising applied voltage. The terminal voltage, after removing the external power source, shows a logarithmic decline, which is theoretically based on the Butler–Volmer equation.

$$U(t) = a - b\ \ln(c + t).$$

For a 24 V bipolar supercapacitor in a 2000 h experiment [7], the constants read $a = 4.2$ V, $b = 0.32$ V, $c = 8.4$ h. Electrolytes purged with

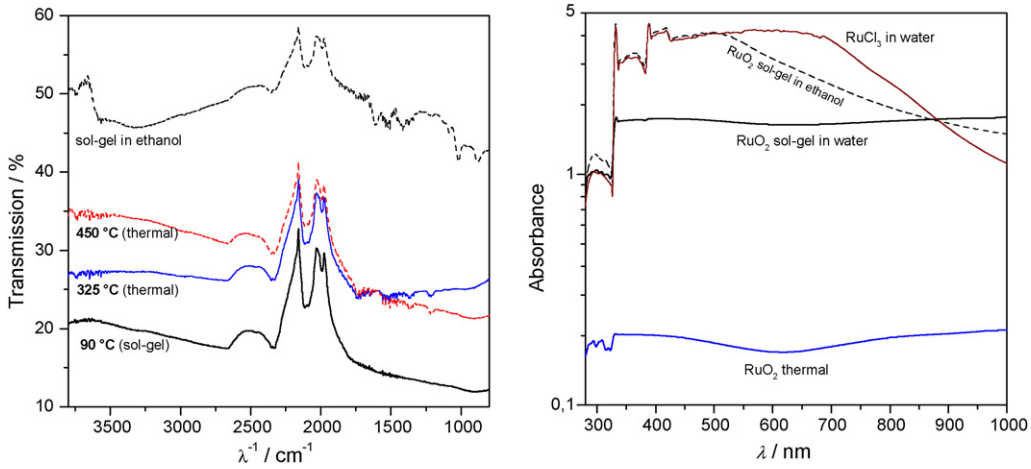

Fig. 13. Spectroscopic characterization of RuO_2 powders prepared by different methods. Left: FTIR spectra of solid powder samples under a diamond ATR unit. Right: UV–vis spectra of dissolved coloured ions above a slurry of metal oxides in water after sedimentation.

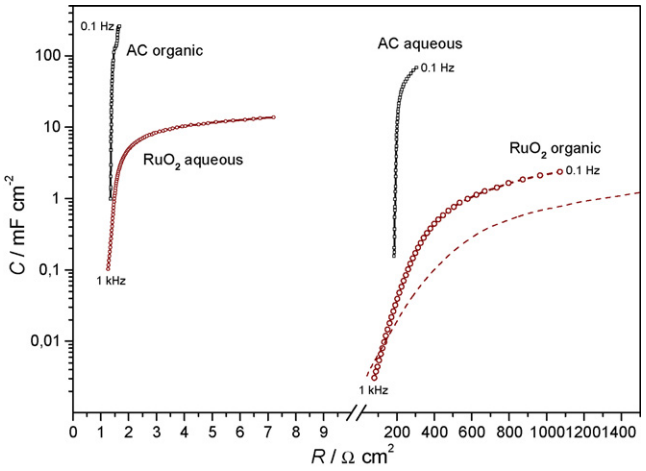

Fig. 14. Impedance spectra, capacitance with respect to resistance, of a cell (cf. Fig. 11) of two activated carbon electrodes and two RuO_2/Ni electrodes, in aqueous solution (0.89% KCl) and organic electrolyte (saturated solution of NEt_4BF_4 in dry acetonitrile), respectively. Dashed: asymmetric cell of RuO_2/Ni and a plane nickel counter electrode.

nitrogen, air and oxygen behave differently and reveal that oxygen diffusion and the recombination of absorbed hydrogen and oxygen play a major role for self-discharge.

This result supports the charge storage mechanism, proposed in Section 3, based on hydrogen and oxygen sorption. A further hint at the hydrogen–oxygen recombination reaction is given by the fact that traces of platinum (being a recombination catalyst) significantly alter the cyclic voltammogram of a RuO_2 electrode, especially in the hydrogen region.

4. Conclusion and summary

1. We were able to reproduce the potential determining proton exchange mechanism at a pH glass electrode by a layer of hydrous platinum metal oxides in a matrix of polymer resin. For potentiometric measurements, RuO_2/nickel electrodes can be combined with a glassy carbon counter electrode.
2. The electrode potential, in acid solution, increases with rising pH, and is formally due to hydrogen oxidation bound in RuO_2. Protons are released by the dissociative adsorption of water and superacid OH groups. Hence, a RuO_2 electrode in acid solution works as a reversible hydrogen electrode.

$$[Ru]_2O + H_2O \rightleftharpoons 2[Ru]OH \text{ or } [RuO]_2(H_2) \rightleftharpoons 2[Ru]O + 2H^+ + 2e^-$$

In alkaline solution, the electrode potential decreases with rising pH, due to the formal reduction of oxygen bound in RuO_2. Actually, by the dissociative adsorption of water, hydroxide sites are formed and bound in ruthenium cluster ions.

$$4[Ru]O \text{ or } 2[Ru]_2(O_2) + 2H_2O + 4e^- \rightleftharpoons 2[Ru]_2O + 4OH^-$$

3. Amorphous $RuO_2{\cdot}xH_2O$ layers, especially produced by alkaline precipitation, exhibit a large amount of grain boundaries which facilitate the admission and dissociative adsorption of water on the surface sites of the deformed rutile lattice. The inner particle volume is slowly accessed by protons (or their carriers).
4. For a high pseudocapacitance a certain amount of Ru(III) in the powder turns out to be useful. Under oxidizing conditions protons are removed from the OH sites, which bind at trivalent ruthenium predominantly: "$HRuO_2$" → $RuO_2 + H^+ + e^-$.
5. The SIMS spectra of sol–gel RuO_2 reveal mass peaks at 133 u and 149 u, which might be attributed to the predominant Ru(III) and Ru(IV) species minus a proton, and cannot be found in single crystalline RuO_2 in this significant amount.
6. RuO_2 electrodes age by partial oxidation of the surface sites, i.e. by a loss of Ru(III) surface sites, which have been shown above to be essential for the dissociative adsorption of water involving proton conductivity.
7. There is a considerable proton exchange between a RuO_2 electrode and the surrounding electrolyte, so that the capacitance at a RuO_2 electrode can be used as a probe for water in organic media.

Acknowledgements

The author wants to appreciate the support by his diligent students U. Bär, Th. Felbinger, M. Fritsch, Ch. Reitmeier, and A. Rothäuger (in alphabetical order).

References

[1] P. Kurzweil, in: J. Garche (Ed.), Encyclopedia of Electrochemical Power Sources, Elsevier, 2008.
[2] B.E. Conway, Electrochemical Supercapacitors, Kluwer Academic/Plenum Publishers, 1999 (Chapter 11).

[3] S. Trasatti, P. Kurzweil, Platinum Met. Rev. 38 (2) (1994) 46.
[4] H.B. Beer, J. Electrochem. Soc. 127 (1980) 303C;
H.B. Beer, Belg. Pat. 710551, 1968.
[5] (a) K. Doblhofer, M. Metikos, Z. Ogumi, H. Gerischer, Ber. Bunsenges. Phys. Chem. 82 (1978) 1046–1050;
(b) M. Metikos-Hukovic, R. Babic, F. Jovic, Z. Grubac, Electrochim. Acta 51 (2006) 1157–1164.
[6] S. Trasatti, G. Lodi, Conductive Metal Oxides, vol. A, Amsterdam, Elsevier, 1980.
[7] (a) P. Kurzweil, O. Schmid, A. Löffler, Proceedings of the 7th International Seminar on Double Layer Capacitors, Deerfield Beach, USA, December 8–10, 1997, pp. 8–10;
(b) P. Kurzweil, O. Schmid, Proceedings of the 6th International Seminar on Double Layer Capacitors, Deerfield Beach, USA, December 9–11, 1996, pp. 9–11.
[8] Long time stable electrode: EP 0622815, DE 4313474, 1994.
[9] S. Sarangapani, P. Lessner, J. Forchione, A. Griffith, A.B. Laconti, J. Power Sources 29 (1990) 355.
[10] Y. Takasu, S. Onoue, K. Kameyama, Y. Murakami, K. Yahikozawa, Electrochim. Acta 39 (13) (1994) 1993–1997.
[11] H. Kim, B.N. Popov, J. Power Sources 104 (2002) 52–61.
[12] J.H. Jang, A. Kato, K. Machida, K. Naoi, J. Electrochem. Soc. 153 (2) (2006) A321–A328.
[13] Y.E. Roginskaya, O.V. Morozova, Electrochim. Acta 40 (7) (1995) 817–822.
[14] R. Koncki, M. Mascini, Anal. Chim. Acta 351 (1997) 143–149.
[15] A.F. Holleman, E. Wiberg, Lehrbuch der Anorganischen Chemie, W. de Gruyter, Berlin, 1995.
[16] A. Patel, D.T. Richens, Inorg. Chem. 30 (20) (1991) 3789–3792.
[17] R.A. Huggins, H. Prinz, M. Wohlfahrt-Mehrens, L. Jörrissen, W. Witschel, Solid State Ionics 70/71 (1994) 417–424.